Supplementary information

RIDME distance measurements using Gd(III) tags with a narrow central transition

A. Collauto[1], V. Frydman[2], M. D. Lee[3], E. H. Abdelkader[4], A. Feintuch[1], J. D. Swarbrick[3], B. Graham[3], G. Otting[4], D. Goldfarb[1]
[1]Department of Chemical Physics and [2]Department of Chemical Research Support, Weizmann Institute of Science, Rehovot 76100, Israel
[2]Monash Institute of Pharmaceutical Sciences, Monash University, Parkville, VIC 3052, Australia
[3]Research School of Chemistry, Australian National University, Canberra, ACT 2601, Australia

Contents

1. Measurements of the temperature-dependent T_M and T_{1e} for the Gd(III)-DOTA ruler

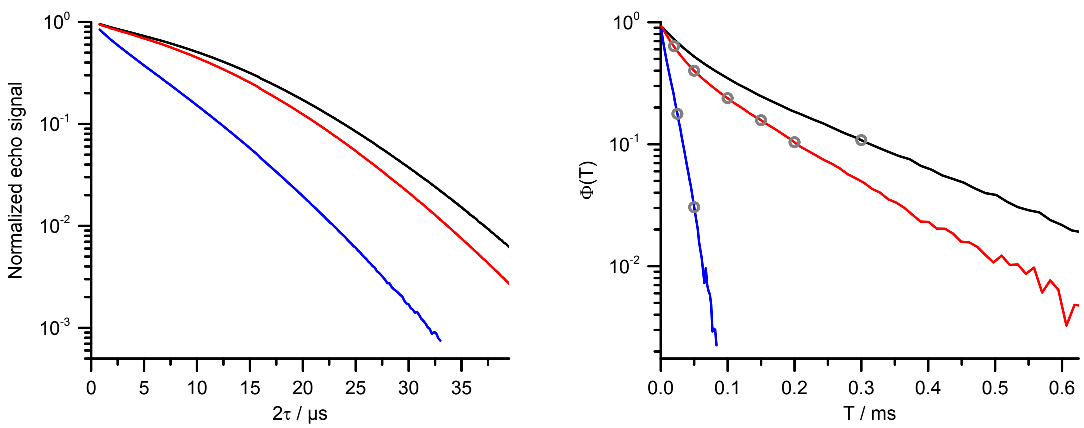

Figure S1. Echo decay traces (a) and SR traces (b) of the Gd(III)-DOTA ruler at 5 K (black), 10 K (red), and 25 K (blue). Circles on the SR traces mark the T_{mix} values used for RIDME experiments. The magnetic field was set to the maximum of the EPR spectrum for both experiments. In (b) $\Phi(T) = 1 - I(T)/I(0)$, where I(T) is the echo intensity at time T and I(0) is the echo intensity corresponding to the equilibrium magnetization.

2. Analysis of background decay and signal-to-noise ratio

Table S1 lists the fraction of spins f_{SR} that recover during the mixing time, T_{mix}, as derived from the saturation recovery curves (Fig. 3b, Fig. S2b), the background fit parameters ($I(t) = e^{-k \cdot t^{d/3}}$) and the signal-to-noise ratio (SNR) for the various measurements carried out on the Gd(III)-DOTA ruler.

The SNR normalized to the acquisition time was evaluated as

$$SNR_{1h} = \frac{\lambda}{\sigma \cdot \sqrt{t}} \qquad \text{(S1)}$$

where λ is the modulation depth, t is the measurement time expressed in hours and σ is the most representative value of the standard deviation of the noise, obtained as the difference between the form factors and the corresponding fits. This approach was possible because very good fits were obtained. Alternatively, the standard deviation could have been derived from the region of the background-subtracted traces, where the modulations have already decayed. This latter approach would have been difficult for the protein samples, where the modulations persisted to the end of the DEER trace.

Evaluation of the SNR requires two clarifications. Firstly, the presence of ^{2}H-ESEEM leads to an overestimation of the effective noise of the trace. Furthermore, when its intensity is affected by experimental parameters such as the field position or pulse length (see Fig. 8 and S7 respectively), only a rough comparison between the SNR for different traces is possible. Secondly, at values of the dipolar evolution time close to zero, the refocused virtual echo (RVE, see Fig. 1b), the refocused stimulated echo (RSE, see Fig. 1b), and the primary echo from the last two pulses of the dead-time free RIDME sequence overlap. The last two are canceled by the phase cycle used while the first echo is retained. For long values of the mixing time, however, the intensity of the primary echo, which does not depend on the mixing time, is orders of magnitude larger than the intensity of the refocused virtual echo, so that a small imperfection in the setup of the pulse phases or even a weak non-linearity of the receiver can lead to incomplete cancelation of the unwanted echoes. This would be manifested by an increase or decrease of the RIDME signal in the $t = 0$ region, hence causing an inaccurate evaluation of the modulation depth. Furthermore, this artifact is not expected to appear as a spike, but rather as a smooth variation of the dipolar evolution trace with the shape of the uncompensated primary echo. In summary, comparison of the SNR is most meaningful only within the series of experiments that involve only a change of T_{mix} and do not involve an adjustment of the power and/or phase of the pulses within the series. On the other hand, neither of these parameters is expected to affect the evaluation of the parameters k and d defining the background function.

Table S1. Summary of the background decay and analysis for the DEER and RIDME experiments performed on the Gd(III)-DOTA ruler.

T (K)	t_π (ns)	T_{mix} (μs)	ΔB_0[1] (mT)	f_{SR}[1]	k[1]	d[1]	λ[1,2]	SNR_{1h}[1,2]	$V_{echo, N}$[1,2]
10	DEER ($t_\pi(\nu_2)$ = 15 ns, Δν = 100 MHz)			---	0.01	3.0	1.8%	36	1.43
5	30	300	0	89%	0.14	4.9	11.4%	71	1.94
10	30	150	0	84%	0.16	4.4	10.4%	75	3.33
10	30	20	0	37%	0.05	5.0	5.7%	39	14.0
10	30	50	0	60%	0.09	4.9	7.4%	57	8.80
10	30	100	0	76%	0.12	4.7	8.6%	59	4.73
10	30	200	0	90%	0.17	4.4	8.2%	53	2.05
10	25	150	0	84%	0.16	4.4	13.4%	85	3.01
10	30	150	0	84%	0.16	4.4	13.7%	113	3.54
10	50	150	0	84%	0.16	4.3	11.3%	126	3.99
10	100	150	0	84%	0.17	4.2	10.0%	195	4.03
10	200	150	0	84%	0.16	4.2	8.3%	129	4.17
10	30	150	0	84%	0.17	4.3	10.5%	56	3.43
10	30	150	-2.5	84%	0.30	3.8	22.5%	59	0.19
10	30	150	-5.0	84%	0.33	3.7	20.8%	48	0.17
10	30	150	-10	84%	0.34	3.7	21.6%	51	0.16
10	30	150	-25	84%	0.34	3.8	22.2%	36	0.10
25	30	25	0	82%	0.11	4.4	7.3%	78	1.40
25	30	50	0	97%	0.15	4.2	8.8%	58	0.54

[1] ΔB_0: magnetic field offset with respect to the maximum of the EPR spectrum. f_{SR}: fraction of spins that recovered during the mixing time. k, d: parameters defining the background function ($I(t) = e^{-k \cdot t^{d/3}}$). λ: modulation depth. SNR_{1h}: signal to noise ratio for 1 h accumulation time. $V_{echo, N}$: intensity of the refocused virtual echo at zero dipolar evolution time normalized by the number of scans and number of shots per point.

[2] From repeated measurements performed on different days under the same experimental conditions we estimate the error in λ, arising primarily from the background fit, to be around

25%, for $V_{echo,\ N}$ to be around 5%, and for the SNR_{1h} to be around 50%. The uncertainty for experiments done all in the same day is lower.

3. Field and temperature dependence of the phase memory and longitudinal relaxation times for the Gd(III)-DOTA ruler

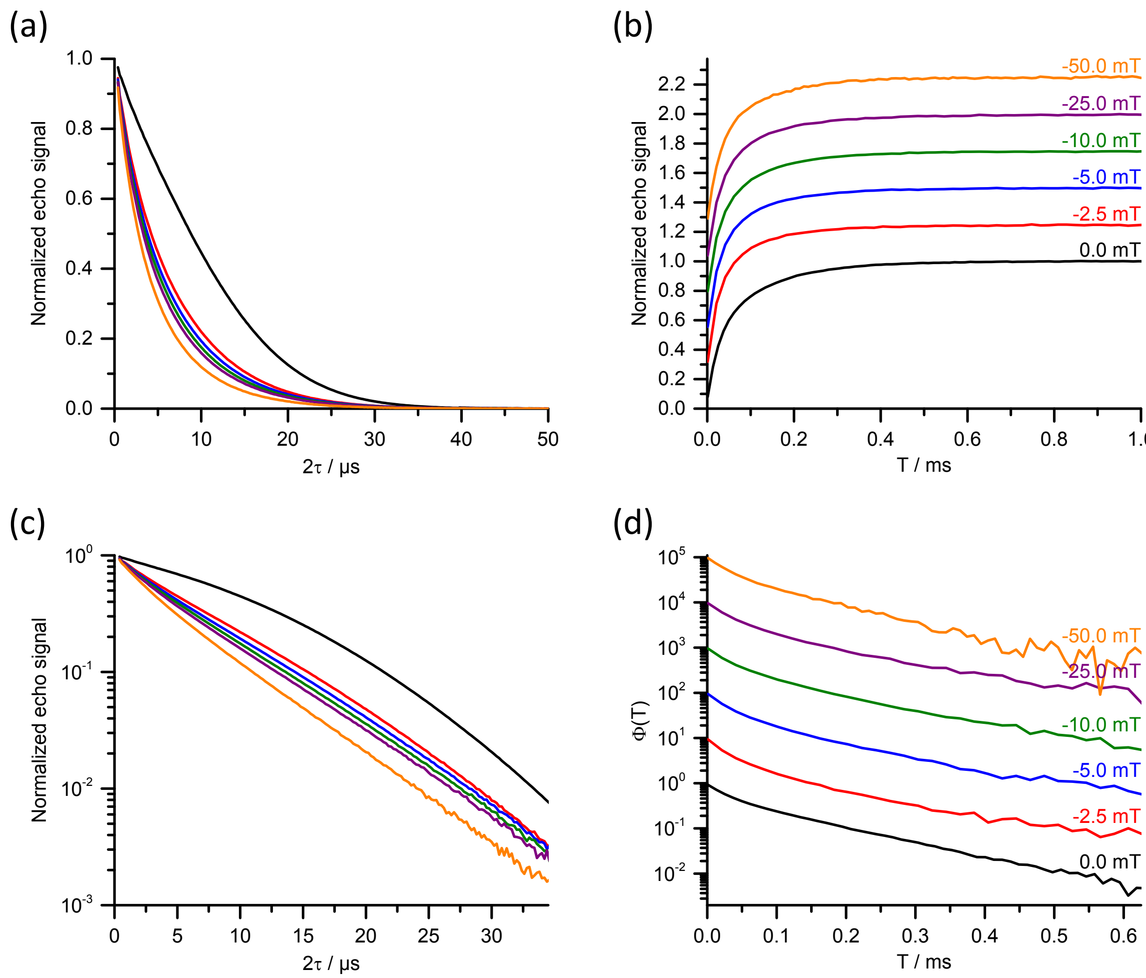

Figure S2. (a, c) Echo decay and (b,d) saturation recovery measurements on the Gd(III)-DOTA ruler performed at 10 K for different magnetic field values ΔB_0 as indicated on the figure, where ΔB_0 is the magnetic field offset with respect to the maximum of the EPR spectrum. In (b) and (d) the traces were shifted with respect to each other for clarity. Φ(T) is defined in Fig. S1.

Table S2. Analysis of the field- and temperature-dependent echo decay curves for the Gd(III)-DOTA ruler (Fig. 3a, Fig. S2a).[a]

		$x_1 = 1.0$		$x_2 = 2.0$		
T	ΔB$_0$	$T_{M,1}$	A_1	$T_{M,2}$	A_2	$T_{M,1/e}$
5 K	0.0 mT	8.33 ± 0.06 µs	48.8 ± 0.2 %	17.12 ± 0.03 µs	51.2 ± 0.2 %	13.5 µs
10 K	0.0 mT	7.52 ± 0.05 µs	53.0 ± 0.2 %	15.48 ± 0.03 µs	47.0 ± 0.2 %	11.9 µs
25 K	0.0 mT	5.359 ± 0.005 µs	100 %	---	0 %	5.1 µs
10 K	-2.5 mT	4.66 ± 0.03 µs	81.2 ± 0.2 %	15.74 ± 0.05 µs	18.8 ± 0.2 %	6.4 µs
10 K	-5.0 mT	4.35 ± 0.02 µs	83.6 ± 0.2 %	15.79 ± 0.06 µs	16.4 ± 0.2 %	5.8 µs
10 K	-10 mT	4.20 ± 0.02 µs	85.5 ± 0.2 %	15.79 ± 0.07 µs	14.5 ± 0.2 %	5.4 µs
10 K	-25 mT	3.90 ± 0.02 µs	86.0 ± 0.2 %	15.53 ± 0.07 µs	14.0 ± 0.2 %	5.0 µs
10 K	-50 mT	3.38 ± 0.02 µs	87.9 ± 0.2 %	14.38 ± 0.07 µs	12.1 ± 0.2 %	4.2 µs

[a] The experimental traces were fitted by a double stretched exponential function $y = A_1 \cdot e^{-\left(\frac{2\tau}{T_{M,1}}\right)^{x_1}} + A_2 \cdot e^{-\left(\frac{2\tau}{T_{M,2}}\right)^{x_2}}$, where x_1 and x_2 were fixed to 1.0 and 2.0, respectively. These values gave a very good fit for all the traces. $T_{M,1/e}$ corresponds to the time at which the echo decayed to 1/*e* of its initial value.

Table S3. Analysis of the field- and temperature-dependent saturation recovery curves for the Gd(III)-DOTA ruler (Fig. 3b, Fig. S2b).[a]

T	ΔB$_0$	Fast component		Slow component			
		$T_{1,f}$	A_f	$T_{1,s}$	A_s	$T_{1,1/e}$	$T_{M,1/e}/T_{1e,1/e}$
5 K	0.0 mT	40.2 ± 1.1 µs	43.5 ± 0.6 %	189.9 ± 2.3 µs	56.5 ± 0.6 %	92.6 µs	0.15
10 K	0.0 mT	25.8 ± 0.6 µs	47.6 ± 0.6 %	129.8 ± 1.6 µs	52.4 ± 0.6 %	57.2 µs	0.21
25 K	0.0 mT	---	0 %	15.10 ± 0.05 µs	100 %	13.2 µs	0.39
10 K	-5.0 mT	25.8 ± 0.6 µs	62.0 ± 0.8 %	124.6 ± 2.8 µs	38.0 ± 0.8 %	45.2 µs	0.13
10 K	-10 mT	25.6 ± 0.7 µs	57.5 ± 0.8 %	124.2 ± 2.5 µs	42.5 ± 0.8 %	50.2 µs	0.11
10 K	-25 mT	28.8 ± 0.7 µs	63.2 ± 0.8 %	137.8 ± 3.1 µs	36.8 ± 0.8 %	50.9 µs	0.10
10 K	-50 mT	26.1 ± 0.6 µs	56.2 ± 0.7 %	120.0 ± 2.0 µs	43.8 ± 0.7 %	49.9 µs	0.08

[a] The experimental traces were fitted to a double exponential function $y = A_f \cdot e^{-\frac{T}{T_{1,f}}} + A_s \cdot e^{-\frac{T}{T_{1,s}}}$. $T_{1e,1/e}$ corresponds to the time at which the echo recovered to (1-1/*e*) of its initial value ($\Phi(T_{1e,1/e}) = 1/e$, see Fig. S1).

4. Analysis of the DEER and RIDME traces for the Gd(III)-DOTA ruler

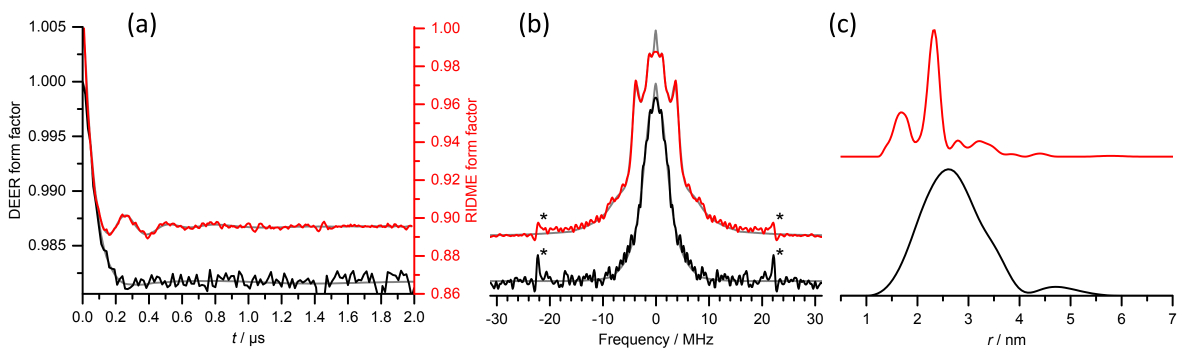

Figure S3. Analysis of the DEER ($\Delta\nu$ = 100 MHz; black) and RIDME (T_{mix} = 150 µs; red) experiments performed at 10 K on the Gd(III)-DOTA ruler shown in Fig. 2a. (a) Form factors and (b) respective frequency spectra (grey lines: Tikhonov regularization). (c) Distance probability distributions. In plots (a), (b), and (c), the results of Tikhonov regularization are shown (DEER: α = 1000; RIDME: α = 1). The signals in the frequency spectra arising from ^{2}H-modulation (ν = ±22.5 MHz) are marked by asterisks (*).

5. Effect of experimental parameters on the RIDME traces of the Gd(III)-DOTA ruler

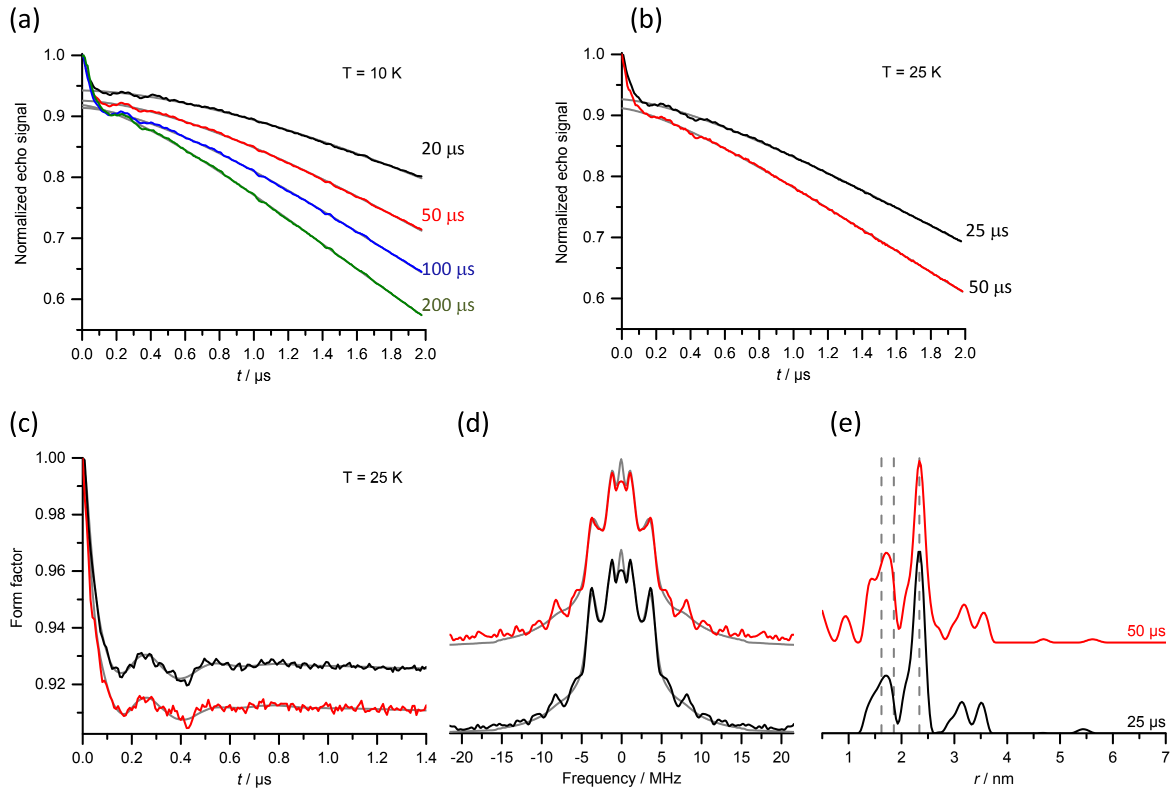

Figure S4. RIDME experiments performed on the Gd(III)-DOTA ruler as a function of T_{mix} (values are indicated on the figure. (a) Dipolar evolution traces measured at T = 10 K. (b) Dipolar evolution traces measured at T = 25 K. Fits of the background signal are displayed in grey in (a) and (b). (c) Form factors measured at 25 K, and best fits (grey). (d) Fourier transforms of the RIDME form factors (black and red) and fits (grey) in (c). (e) Distance distributions obtained from Tikhonov regularization of the RIDME form factors (α = 1) in (c). The grey dashed lines denote, from right to left, the mean distances corresponding to the first, second, and third harmonic of the electron-electron dipolar interaction. The analysis of the traces displayed in (a) is presented in Fig. 7 in the main text.

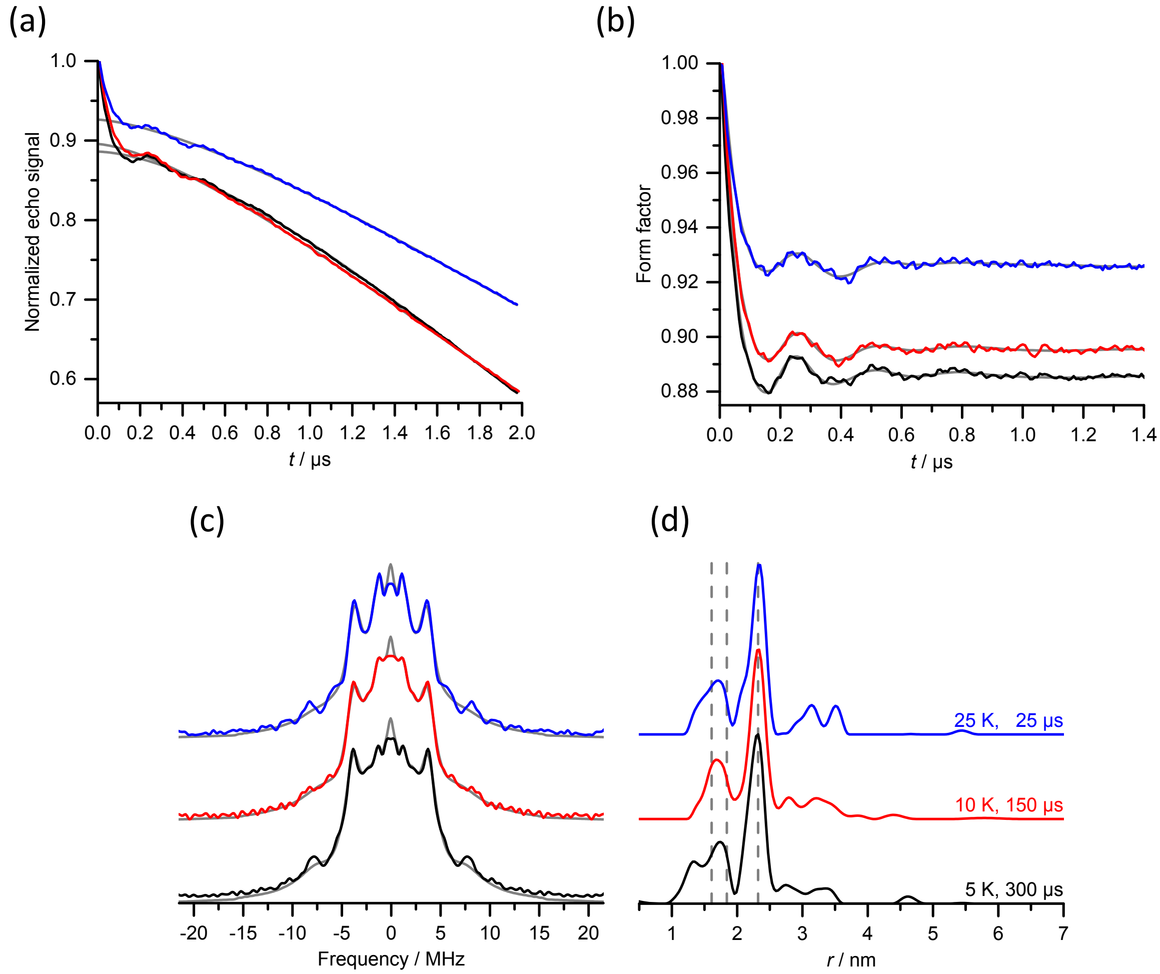

Figure S5. RIDME experiments of the Gd(III)-DOTA ruler as a function of the temperature under conditions of constant fraction (≈ 85%) of spins that recovered during the mixing time. (a) Dipolar evolution traces recorded using the parameters indicated in the figure. Fits of the background signal are displayed in grey. (b) Form factors (colored) and fits (grey). (c) Fourier transforms of the RIDME form factors (colored) and fits (grey). (d) Distance distributions obtained from Tikhonov regularization of the RIDME form factors (α = 1). The grey dashed lines denote, from right to left, the mean distances corresponding to the first, second, and third harmonic of the electron-electron dipolar interaction. The same color codes are used for all panels.

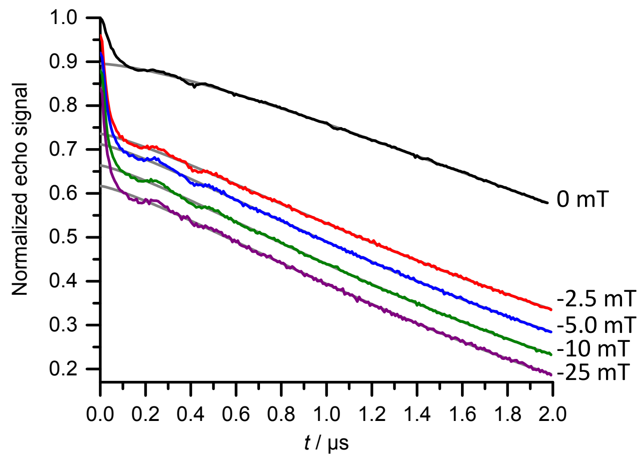

Figure S6. Dipolar evolution traces for the RIDME experiments performed on the Gd(III)-DOTA ruler as a function of the magnetic field offset with respect to the maximum of the EPR spectrum, ΔB_0, as noted on the figure. The data were recorded at T = 10 K with T_{mix} = 150 µs. Fits of the background signal are shown in grey. Each trace was displaced downwards by an additional 0.04 units for improved visibility.

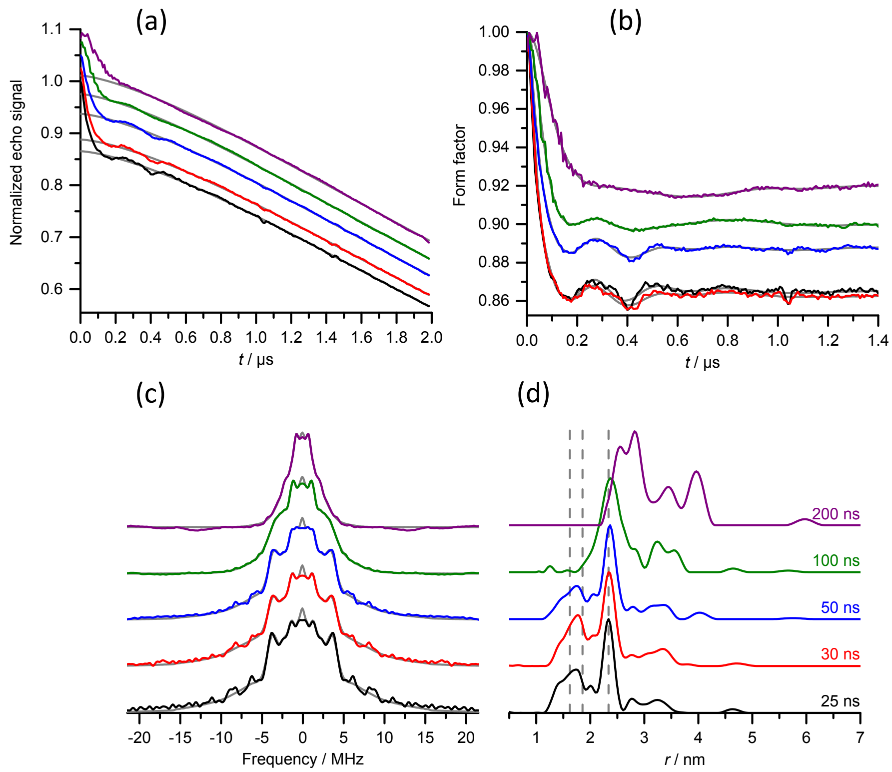

Figure S7. RIDME experiments of the Gd(III)-DOTA ruler at different pulse excitation bandwidths. (a) Dipolar evolution traces recorded at T = 10 K with T_{mix} = 150 µs, using t_π as indicated on the figure and $t_{\pi/2} = t_\pi/2$. Fits of the background signal are shown in grey. (b) Form factors (colored) and fits (grey). (c) Fourier transforms of the RIDME form factors (colored) and fits (grey) in (b). (d) Distance distributions obtained from Tikhonov regularization of the RIDME form factors (α = 1). The grey dashed lines denote, from right to left, the mean distances corresponding to the first, second, and third harmonic of the electron-electron dipolar interaction. The same color codes are used for all panels.

6. Field-swept echo-detected EPR spectrum of the C9-Gd(III) tag

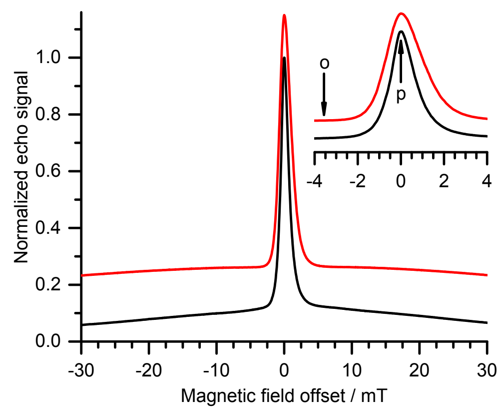

Figure S8. W-band Echo-detected EPR spectra of the Gd(III)-DOTA dimer (black) and of the ERp29 S114C-C9-Gd(III) homodimer (red) recorded at 10 K. The inset shows a magnification of the central transition region, where the "p" and "o" labels denote the positions of the pump and observe pulses in the DEER experiment, respectively. The traces were displaced in the vertical direction for improved visualization.

7. Dipolar evolution traces for the DEER and RIDME experiments on the mutants of the ERp29 homodimer labeled with the C9-Gd(III) tag

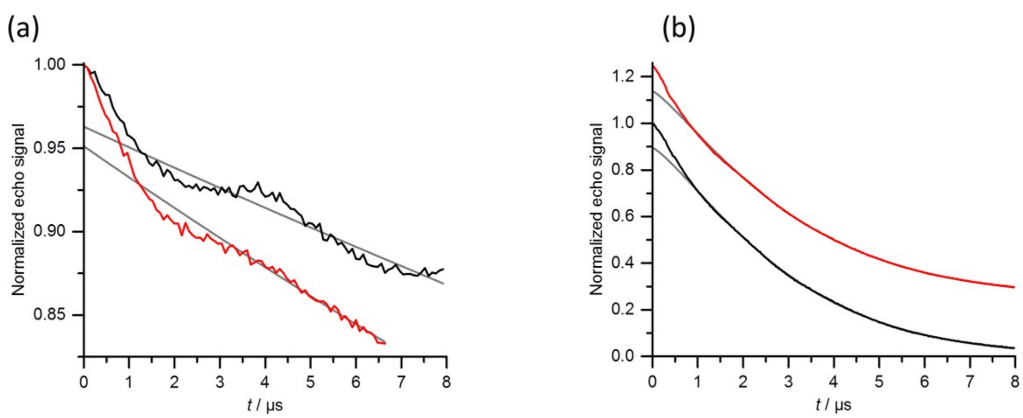

Figure S9. Dipolar evolution traces recorded at 10 K on 100 μM solutions of the ERp29 mutants S114C (black) and G147C (red). (a) DEER experiments. The pump pulse was set at the maximum of the EPR spectrum with a length of 15 ns. The frequency difference between the pump and observe pulses was 100 MHz. (b) RIDME experiments. The mixing time was set to 25 µs and the experiments were performed at the maximum of the EPR spectrum. The RIDME traces were displaced in the vertical direction for improved visualization.

8. Effect of experimental parameters on the RIDME traces for the S114C mutant of the ERp29 homodimer labeled with the C9-Gd(III) tag

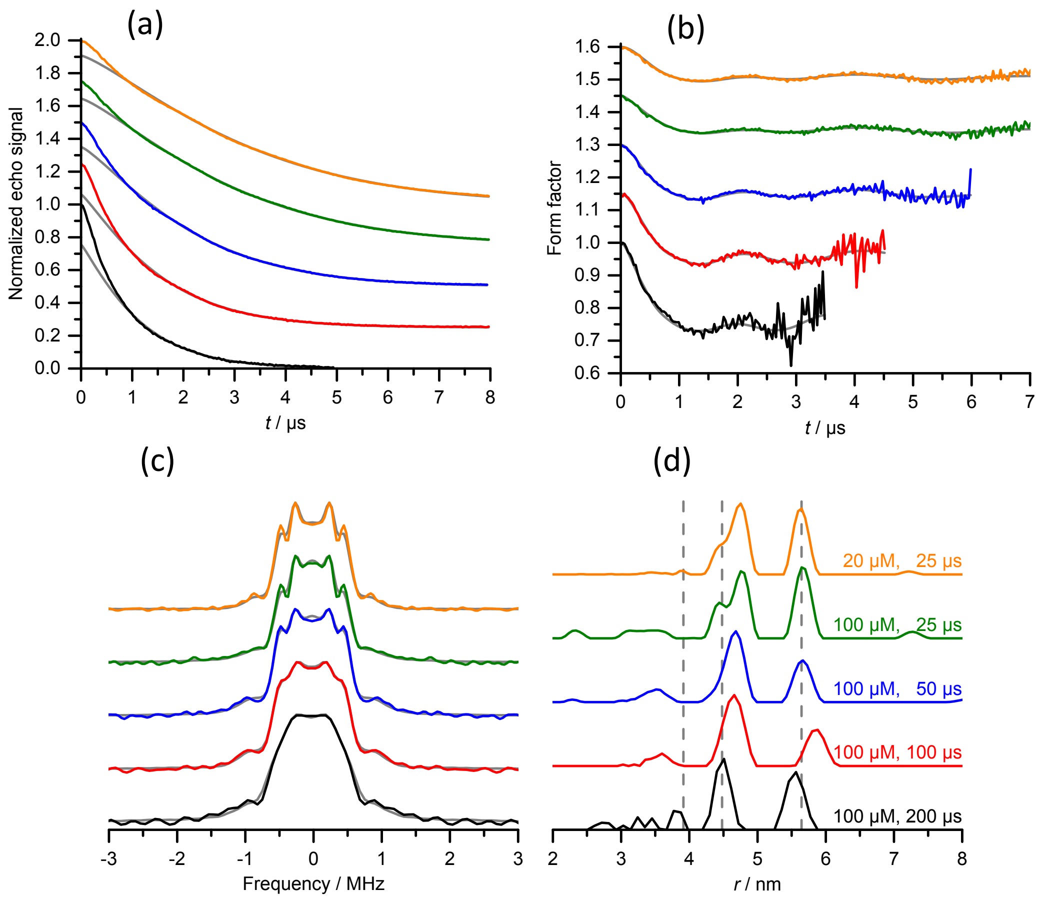

Figure S10. Effect of the mixing time and sample concentration on the RIDME dipolar evolution trace for the S114C mutant of the ERp29 homodimer recorded at 10 K for conditions of concentration and mixing time as indicated on the figure. (a) Dipolar evolution traces (colored) and background fits (grey). (b) Form factors (colored) and fits (grey). (c) Frequency spectra of form factors (colored) and fits (grey). (d) Distance probability distribution curves obtained from Tikhonov regularization of the RIDME form factors (α = 10). The grey dashed lines denote, from right to left, the mean distances corresponding to the first and second harmonic of the electron-electron dipolar interaction. The same color codes are used for all panels.

Table S4. Summary of the background analysis for the DEER and RIDME experiments performed on the ERp29 mutants.

Mutant	Conc. (μM)	T_{mix} (μs)	f_{SR}[1]	k[1]	d[1]	$t_{5\%}$[1] (μs)	λ[1,2]	SNR_{1h}[1,2]	$V_{echo, N}$[1,2]
S114C	100	DEER	---	0.013	3.0	---	3.6%	6	0.02
S114C	100	25	31%	0.232	3.8	7.3	10.8%	22	0.39
S114C	100	50	48%	0.359	3.7	5.3	15.3%	28	0.29
S114C	100	100	66%	0.573	3.5	3.9	20.0%	22	0.18
S114C	100	200	83%	0.827	3.4	2.8	25.2%	18	0.08
S114C	20	25	30%	0.210	3.8	7.9	9.6%	10	0.13
G147C	100	DEER	---	0.020	3.0	---	4.8%	9	0.02
G147C	100	25	35%	0.231	3.7	7.8	11.0%	45	0.41

[1] f_{SR} is the fraction of spins that recovered during the mixing time, k and d are the parameters defining the background function ($I(t) = e^{-k \cdot t^{d/3}}$), $t_{5\%}$ is the maximum RIDME dipolar evolution time for which the raw signal is above 5% of its initial value, λ is the modulation depth, SNR_{1h} is the signal-to-noise ratio normalized to 1 hour acquisition time, and $V_{echo, N}$ is the intensity of the refocused virtual echo at zero dipolar evolution time normalized by the number of scans and number of shots per point.

[2] The estimates of the errors on λ, SNR_{1h} and $V_{echo, N}$ are the same as in Table S1.

9. Mutant and concentration dependence of the phase memory and longitudinal relaxation times for the C9-Gd(III)-labeled ERp29 samples

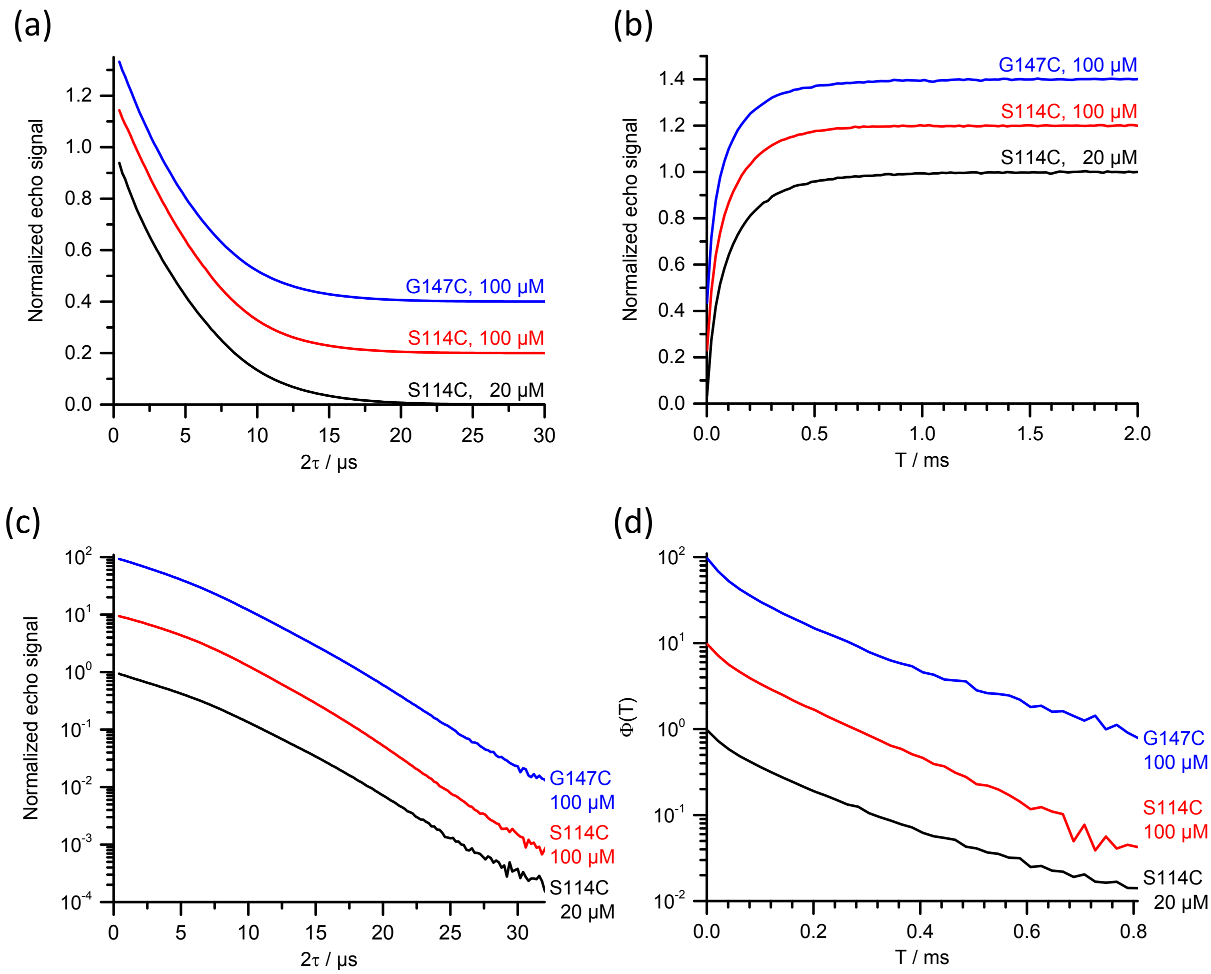

Figure S11. (a,c) Echo decay and (b,d) saturation recovery curves of the ERp29 S114C-C9-Gd(III) and G147C- C9-Gd(III) mutants. The data were recorded at 10 K at the maximum of the EPR spectrum. Black and red: S114C mutant at a concentration of 20 µM and 100 µM homodimer, respectively. The traces have been displaced in the vertical direction for improved visualization.

Table S5. Analysis of the mutant- and concentration-dependent echo decay curves for the ERp29 samples (Fig. S11a,c).[a]

		$x_1 = 1.0$		$x_2 = 2.0$		
Mutant	Conc.	$T_{M,1}$	A_1	$T_{M,2}$	A_2	$T_{M,1/e}$
S114C	20 μM	4.27 ± 0.01 μs	71.0 ± 0.1 %	8.33 ± 0.02 μs	29.0 ± 0.1 %	5.7 μs
S114C	100 μM	4.32 ± 0.01 μs	63.6 ± 0.1 %	7.62 ± 0.01 μs	36.4 ± 0.1 %	5.8 μs
G147C	100 μM	4.29 ± 0.01 μs	72.6 ± 0.1 %	7.65 ± 0.02 μs	27.4 ± 0.1 %	5.5 μs

[a] $T_{M,1/e}$ is defined in Table S2.

Table S6. Analysis of the mutant- and concentration-dependent saturation recovery curves for the ERp29 samples (Fig. S11b,d).[a]

		Fast component		Slow component			
Mutant	Conc.	$T_{1,f}$	A_f	$T_{1,s}$	A_s	$T_{1e,1/e}$	$T_{M,1/e}$ / $T_{1e,1/e}$
S114C	20 μM	36.1 ± 1.2 μs	41.7 ± 0.7 %	182.8 ± 2.4 μs	58.3 ± 0.7 %	98.4 μs	0.06
S114C	100 μM	28.9 ± 0.6 μs	36.5 ± 0.4 %	151.9 ± 0.9 μs	63.5 ± 0.4 %	88.9 μs	0.07
G147C	100 μM	32.6 ± 0.9 μs	48.9 ± 0.7 %	168.1 ± 2.5 μs	51.1 ± 0.7 %	77.8 μs	0.07

[a] $T_{1e,1/e}$ is defined in Table S3.